Topology Design and Optimization of Modular Soft Robots Capable of Homogenous and Heterogenous Reconfiguration

Caitlin Freeman
Agile Robotics Lab,
Department of Mechanical Engineering,
University of Alabama,
Tuscaloosa, AL 35487
e-mail: clfreeman7@crimson.ua.edu

Justin Conzola
Agile Robotics Lab,
Department of Mechanical Engineering,
University of Alabama,
Tuscaloosa, AL 35487
e-mail: jhconzola@crimson.ua.edu

Vishesh Vikas
Agile Robotics Lab,
Department of Mechanical Engineering,
University of Alabama,
Tuscaloosa, AL 35487
e-mail: vvikas@ua.edu

The deformability of soft material robots provides them with the ability to transform between complex shapes and forms. This unique ability facilitates Modular Soft Robots (MSoRos) to assemble and reconfigure into different configurations, e.g., planar and spherical. These topologies display widely different locomotion modes that are desirable to navigate different environments, e.g., crawling or rolling for these cases. This research presents topology design and optimization methodology of MSoRos capable of both homogeneous and heterogeneous reconfiguration in spherical and planar configurations. Homogeneous reconfiguration refers to the scenario when all the modules are identical, while the heterogeneous contains nonidentical modules. The sequential design approach uses a polyhedron (Archimedean or Platonic) as the base solid to define module characteristics. As the design processes involve nonlinear projections, the base polyhedron also dictates the type of reconfiguration—heterogeneous (Archimedean) or homogeneous (Platonic). Thereafter, it applies the polyhedron vertex alignment principle to ensure geometric alignment of the modules during reconfiguration. Planar and spherical distortion metrics are defined to quantify distortions due to reconfiguration. Subsequently, the optimal topology is obtained by minimizing a cost function that is a weighted sum of the two distortion metrics. The result is a set of MSoRos capable of distinct 1D and 2D planar configurations (both heterogeneous and homogeneous) and multiple 3D spherical configurations of varying radii (both heterogeneous and homogeneous). The methodology is validated on a MSoRo system based on the combination of a cuboctahedron (Archimedean solid) and a cube and an octahedron (Platonic solids). [DOI: 10.1115/1.4062265]

1 Introduction

Roboticists have long looked to nature for inspiration to make robots that are more versatile, adaptable, and resilient. Many robotic systems incorporate biological features, simulating swarm behavior or shape-morphing ability. For example, armadillos and pangolins perform legged locomotion, but can roll into a ball for self-defense. This reconfiguration ability inspires modular robots that are capable of group behavior (e.g., rolling) entirely distinct from any individual capability (e.g., walking) [1–5]. This increased versatility has motivated a large field of research, typically constrained to rigid robots and conventional joints [6–8]. The advent of soft materials in the field of robotics allows for change in the shape of the robot modules that has potential to further exploit the dynamics of the reconfigured system. As an example, the locomotion dynamics of a planar robot (2D) are different from that of a series of them connected in a caterpillar-like configuration (1D) or a spherical ball (3D), Fig. 1. This is due in part to the changing amount of area of contact with the environment. The research into topology and morphology design of modular soft robots is very recent, with the primary focus on the modular nature of the robotic system [9–11]. However, mathematically, soft materials afford topological advantages. One may observe the example of spherical reconfiguration, i.e., reconfiguration of a set of Modular Soft Robots (MSoRos) into a sphere configuration, where their default state is the planar configuration, Fig. 1. The cartography analogy of this process is that of flattening a sphere onto a planar map [12]. This cannot be achieved without distortions, as per Gauss' Theorema Egregium. It states that the Gaussian curvature of a surface does not change if one bends the surface without stretching it; a cylindrical tube can be unrolled onto a plane as they both have curvature of zero. However, a sphere of radius R having positive curvature of $1/R^2$ cannot be flattened onto a plane without distorting distances and/or shapes.

The design of spherical "modules" is the equivalent of spherical tessellation widely explored in art by Escher [13]. To make this process possible using materials with approximately zero curvature, Delp et al. [14] describe a process, inspired by clothing design, of smoothing an octahedron to form a round sphere. These concepts can be borrowed and adapted to perform analytical parametric design optimization of the MSoRo topology. This is contrasted with the more popular but costly finite element method-based design optimization of soft robots [15]. Recently, Freeman et al. [16] have

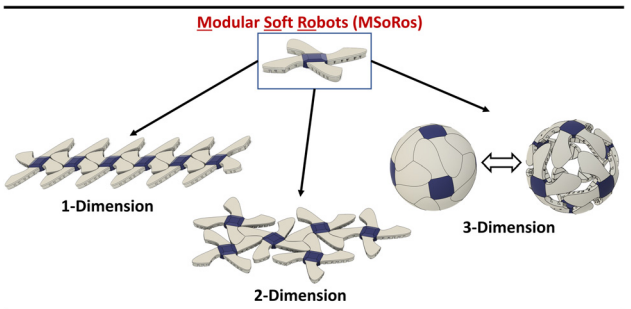

Fig. 1 Dimensional change capability of homogeneous MSoRos

Manuscript received June 16, 2022; final manuscript received March 28, 2023; published online April 28, 2023. Assoc. Editor: Charles J. Kim.

investigated the topology design of homogeneous three, four or five-limb MSoRos that can reconfigure into a sphere. This design methodology is based on the five Platonic solids (which have identical polygonal faces) where the number of faces and edges per face correspond to the number of required modules for reconfiguration and module limbs, respectively. For example, a robot designed with the cube as the base Platonic solid results in a four-limb (equal to the number of square edges) MSoRo where six (the number of cube faces) modules are required for reconfiguration into a sphere. The work experimentally validates the ability of an MSoRo to (1) achieve locomotion using motor-tendon actuators in a single module and (2) compensate for topological distortion to realize linear (1D), planar (2D), and spherical (3D) configurations. However, this reconfiguration is limited to homogeneous (identical-face) modules and to a spherical reconfiguration of only one set radius.

Contributions: This research builds on our prior work to extend the topology design and optimization to heterogeneous MSoRos, e.g., three-limb *and* four-limb that can reconfigure collectively into a heterogeneous sphere. Furthermore, they should possess the capability of homogeneous spherical homogeneous reconfiguration, e.g., reconfiguration into one sphere of exclusively three-limb MSoRos *and* another of exclusively four-limb MSoRos. This is done by exploring the topology design and optimization of MSoRos using one of six possible Archimedean solids as the base polyhedron. Archimedean solids are made up of at least two types of regular polygonal faces and can therefore be used as a geometrical basis for a set of heterogeneous MSoRos (i.e., MSoRos with at least two different module shapes). This allows for a higher number of modular reconfigurations resulting in increased locomotive versatility and robustness of the set. The summary of the design methodology is visualized in Fig. 2. The topology is determined by the selection of one Archimedean solid and two or more Platonic solids, as well as an odd-function module topology curve (MT-curve); the use of an odd function for the MT curve drawn tangent to a polyhedral edge ensures isohedral spherical tiling. Each Archimedean solid presents a unique multimodule assembly, enabling MSoRo systems of varying spherical radii and number of modules. This methodology is divided into the forward design (to construct the planar module topologies by modeling and subsequently projecting spherical configuration(s)) and the inverse design (to model the additional spherical configuration(s) from the planar configurations). The forward design is adapted from our previous work [16] and extended to generalize to heterogeneous MSoRos. The final spherical topology is then obtained via an inverse azimuthal equidistant projection onto the tangent plane of the new sphere.

As the robot is expected to deform to achieve change in curvature between spherical and planar configurations, planar and spherical distortion metrics are defined to quantify reconfiguration difficulty. These distortions metrics model the gaps and overlapping area between adjacent modules in heterogeneous and homogeneous configurations normalized to the areas of the modules. The weighted cost function incorporating both distortion metrics is then minimized to find the optimal topologies. As the design processes is nonlinear, the selection of a Platonic solid as the starting polyhedron (i.e., the decision to use a Platonic solid for homogeneous forward design as opposed to an Archimedean solid for heterogeneous forward design) is significant and motivated by the results shown in the paper. The optimal MT curves are found for an MSoRo system based on the hexahedron (cube) and octahedron as the Platonic solids and the cuboctahedron as the Archimedean solid. The results are validated in both MATLAB simulations and experiments (silicone casting of the modules). To find the best possible set of heterogeneous reconfigurable MSoRos, a set with homogeneous forward design based on Platonic solids and inverse design based on an Archimedean solid is compared to a set with heterogeneous forward design based on an Archimedean solid and inverse design based on Platonic solids.

The paper is structured as follows: Sec. 2 describes the forward topology design. Section 3 outlines the inverse topology design. The technique for optimizing the amplitude of the module topology curve is presented in Sec. 4. Section 5 presents the results of the optimization and defines the ideal MT-curve amplitude derived from the cost function. This also includes figures of the simulated distortions and experimental distortions. Finally, Sec. 6 is a discussion of the results and potential future work.

2 Forward Module Topology Design

The overall module topology design methodology is a sequential process that involves (1) selection of the base polyhedra (one Archimedean solid and two or more Platonic solids), (2) selection of the module-topology curve (MT-curve) drawn on the topology plane, (3) generation of the spherical module topology through inverse orthographic projection of the MT-curve onto the circumscribing sphere, (4) construction of the planar module topology using azimuthal equidistant projection of the spherical topology onto the tangent plane, and (5) the generation of an additional spherical module topology via inverse azimuthal equidistant projection and polyhedral vertex alignment. Steps 1–4 in this process collectively comprise the forward design, Fig. 2, while step 5 refers to the inverse design (explored in Sec. 3). *Forward design* is

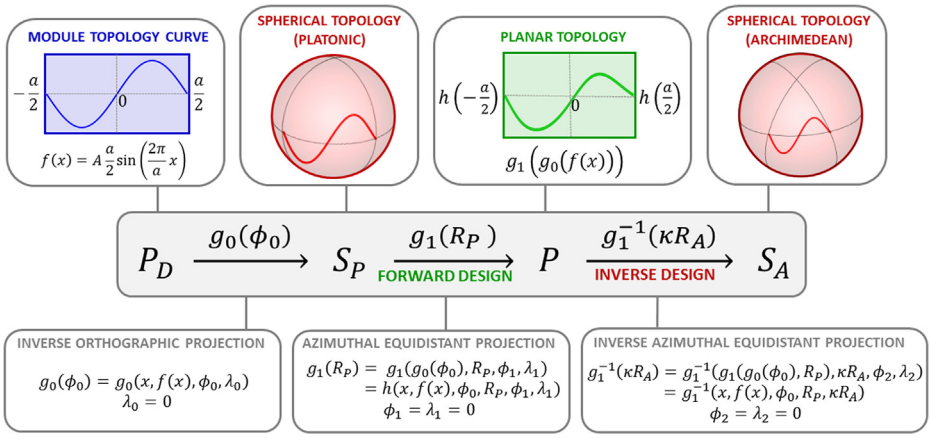

Fig. 2 The flow of the design methodology consists of a sequence of transformations. The design space in the plane P_D undergoes an inverse orthographic projection g_0 to transform into the spherical surface topology space S_P for a Platonic solid (homogeneous). An azimuthal equidistant projection g_1 transforms this into the planar topology space P which defines the MSoRo module shape. Finally, an inverse azimuthal equidistant projection g_1^{-1} this space into the spherical surface topology space S_A for an Archimedean solid (heterogeneous).

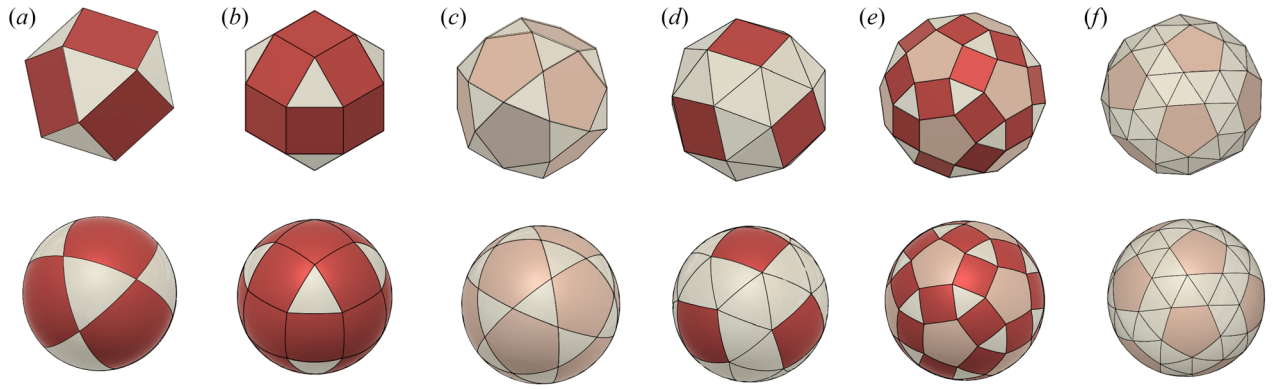

Fig. 3 Six selected Archimedean solids with their corresponding spherical tesselations. The solids are (*a*) cuboctahedron, (*b*) small rhombicuboctahedron, (*c*) icosadodecahedron, (*d*) snub cube, (*e*) small rhombicosadodecahedron, and (*f*) snub dodecahedron.

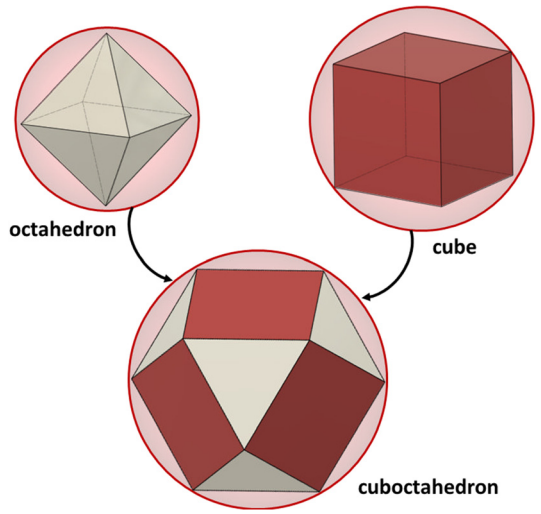

Fig. 4 A cube and an octahedron can be reconfigured to form a cuboctahedron. The spheres in this figure are scaled to show the differences in radii of the circumscribing spheres.

the process of designing the spherical (S) topology of a module for a given MT-curve (design space P_D) and using it to generate the module's planar topology (P). Conversely, *inverse design* is the process of obtaining the spherical configuration (S) from the planar configuration (P), Fig. 2.

For both these processes, the base polyhedra determine the projection details. The forward design can either model homogeneous (based on Platonic solids) or heterogeneous reconfiguration (based on an Archimedean solid). Figure 2 presents homogeneous forward design; the flowchart for heterogeneous forward design would be identical, except for the swapping of the positions of the Platonic (S_P) and Archimedean (S_A) solids. While both methodology flows result in multiple planar modules capable of both heterogeneous and homogeneous planar and spherical reconfiguration, the resulting configurations are different due to the nonlinearity of the design process. The presented framework is generic in which both homogeneous and heterogeneous forward design are defined, analyzed, and later compared (Sec. 5). Homogeneous forward design essentially consists of multiple applications of the Platonic solid-based methodology explored in [16]. Here, we present the generalization of this method for both homogeneous and heterogeneous forward design.

2.1 Selection of Base Polyhedra. While there exist thirteen Archimedean solids, only six exclusively contain faces that are present in Platonic solids. Therefore, this methodology is limited to these six Archimedean solids presented in Fig. 3.

For this discussion, we consider the example of a set of heterogeneous MSoRos based on a cuboctahedron, which has fourteen faces: six squares and eight triangles. We then define the corresponding Platonic solids to be a cube and an octahedron, Fig. 4. Consequently, this MSoRo design will result in fourteen modules: eight three-limb modules based on the triangular faces and six four-limb modules based on the square faces. Individually, the six four-limb MSoRos and eight three-limb MSoRos can reconfigure into two different spheres. The resulting MSoRo system will therefore be capable of both heterogeneous and homogeneous planar and spherical configurations. Moreover, the two radii, $\{R'_1, R'_2\}$, of the homogeneous spherical configurations (cube, octahedron-based) will differ from the radius of the heterogeneous spherical reconfiguration (cuboctahedron-based), R.

While the cuboctahedron is chosen as an example in this paper to elucidate the principles, any of the six Archimedean solids presented here may be chosen. The characteristics of the MSoRo system are then determined by the characteristics of the selected Archimedean solid, shown in Table 2 and its corresponding Platonic solids, shown in Table 1. For both homogeneous and heterogeneous spherical configurations, the number of faces F of the base polyhedron is equal to the number of modules comprising the sphere and the circumradius R is equal to the radius of the sphere. The number of edges per module p is proportional to the number of limbs on each module and is determined by the number of zero-crossings of the MT-curve. However, in this work we limit the MT-curve to have only three zero-crossings for simplicity. Therefore, the number of edges per module p is equal to the number of limbs on each module. The selection of the Archimedean solid automatically determines the Platonic solids, as the number of edges per face must correspond. Finally, Archimedean solids with more than one unique edge type are expected to present more difficult reconfiguration.

2.2 Module Topology Curve. The module topology curve (MT-curve) $f(x)$ determines the module shape. This curve is a function of a polyhedral edge of length a and must be an odd function coinciding with the edge vertices at the ends

$$f(x) = f(-x), \quad s.t. \quad f\left(\frac{a}{2}\right) = f\left(-\frac{a}{2}\right) = 0 \tag{1}$$

There are infinite choices that satisfy these constraints. However, for this discussion we consider the family of sinusoidal functions, i.e.

$$f(x) = A\frac{a}{2}\sin\left(\frac{2\pi}{a}x\right) \tag{2}$$

for a given MT-curve amplitude $A \in [-1, 1]$. This family of curves is chosen because it is smooth, mathematically simple, and contains

Table 1 Characteristics for Platonic solids. *F* is the number of faces, *E* is the number of edges *p* is the number of edges per face, *q* is the number of faces that meet at a vertex, *R*/*a* is the ratio of the circumradius *R* to the edge length *a*, ϕ_0 is the face-center-edge angle, β is the face center to vertex angle.

Solid	F	E	p	q	R/a	ϕ_0	β
Tetrahedron	4	6	3	3	$\frac{\sqrt{6}}{4}$	$\frac{\cos^{-1}\left(\frac{-1}{3}\right)}{2}$	$\cos^{-1}\frac{1}{3}$
Cube	6	12	4	3	$\frac{\sqrt{3}}{2}$	$\frac{\pi}{4}$	$\cos^{-1}\frac{1}{\sqrt{3}}$
Octahedron	8	12	3	4	$\frac{\sqrt{2}}{2}$	$\frac{\cos^{-1}\left(\frac{1}{3}\right)}{2}$	$\cos\ -1\frac{\sqrt{6}}{3}$
Dodecahedron	12	30	5	3	$\frac{\sqrt{15}+\sqrt{3}}{4}$	$\frac{\cos^{-1}\left(\frac{-\sqrt{5}}{3}\right)}{2}$	$\cos^{-1}\sqrt{\frac{5+2\sqrt{5}}{15}}$
Icosahedron	20	30	3	5	$\frac{\sqrt{10+2\sqrt{5}}}{4}$	$\frac{\cos^{-1}\left(\frac{-\sqrt{5}}{5}\right)}{2}$	$\cos^{-1}\sqrt{\frac{74+60\sqrt{2}}{30+6\sqrt{5}}}$

Table 2 Characteristics for Archimedean solids made up of exclusively faces that also occur in Platonic solids. *F* is the number of faces, *E* is the number of edges *p* is the number of edges per face, *q* is the number of faces that meet at a vertex, *R*/*a* is the ratio of the circumradius *R* to the edge length *a*, *i* is the number of unique edges types

Solid	F	E	p	q	R_0/a	i
Cuboctahedron	{8, 6}	14	{3, 4}	4	1	1
Small rhombicuboctahedron	{8, 18}	48	{3, 4}	4	$\frac{\sqrt{5+2\sqrt{2}}}{2}$	2
Icosidodecahedron	{20, 12}	60	{3, 5}	4	$\frac{1+\sqrt{5}}{2}$	1
Snub cube	{32, 6}	60	{3, 4}	5	1.3437	2
Small rhombicosidodecahedron	{20, 30, 12}	120	{3, 4 5}	4	$\frac{\sqrt{11+4\sqrt{5}}}{2}$	2
Snub dodecahedron	{80, 12}	150	{3, 5}	5	2.1558	2

one maxima and one minima on along its domain $x \in [-a/2, a/2]$. Thus, each module will have the same number of legs as the number of edges of the base polyhedron face p. This curve lies on the topology curve plane, Fig. 5.

2.3 Geometry of Projection Planes. Forward design consists of a series of projections that are made with respect to two projection planes: the *topology curve plane* and the *tangent plane*, as shown on a cuboctahedron in Fig. 5. The *topology curve plane* lies coincident to the polyhedral edge and tangent to the vector joining the solid's center and the polyhedral edge midpoint. The *tangent plane* lies tangent to the solid's circumscribing sphere and parallel to a polyhedral face. These two planes are related by a constant angle ϕ_0 determined by the base solid (e.g., octahedron, cube, or octahedron); this constant angle is subsequently incorporated into the projections. This angle ϕ_0 is equal to the face-center-edge angle of the solid, the central angle whose sides intersect the center of a polyhedral face and its adjacent edge midpoint. Note that Archimedean solids will have multiple face-center-edge angles as each solid will have a unique angle ϕ_0 for every unique face. Another significant angle is the face-center-vertex angle β, the central angle whose sides intersect the center of a polyhedral face and its adjacent vertex. The great-circle distance of β equals the preserved azimuthal distance in the second projection in the forward design. The angles ϕ_0 and β are used ensure proper tessellation of the spherical topology in the forward design and vertex alignment in the inverse design, respectively.

Platonic solids have perfect symmetry in their faces, edges, and vertices and therefore have common radii and angles at every edge. The angles ϕ_0 and β for Platonic solids are listed in Table 1. Archimedean solids, however, posses only vertex symmetry. Thus, each unique Archimedean face with p edges has unique angles $\phi_{0,p}$ and β_p. These can be found via trigonometric equations in terms of the circumradius R, the edge length a, and the apothem e_p for a given p-gon face:

$$\phi_{0,p} = \cos^{-1}\left(\frac{\sqrt{R^2-(a/2)^2-e_p^2}}{\sqrt{R^2-(a/2)^2}}\right), \qquad \beta_p = \cos^{-1}\left(\frac{\sqrt{R^2-(a/2)^2-e_p^2}}{R}\right) \tag{3}$$

Apothem lengths for face shapes that occur in Platonic solids are listed in Table 3.

2.4 Forward Spherical Topology. The forward spherical topology is obtained through an inverse orthographic projection of the MT-curve $f(x)$ drawn on the *topology curve plane* onto the circumscribing sphere of radius R. The latitude and longitude of the projection (ϕ, λ) originating from (ϕ_0, λ_0) are generically defined as

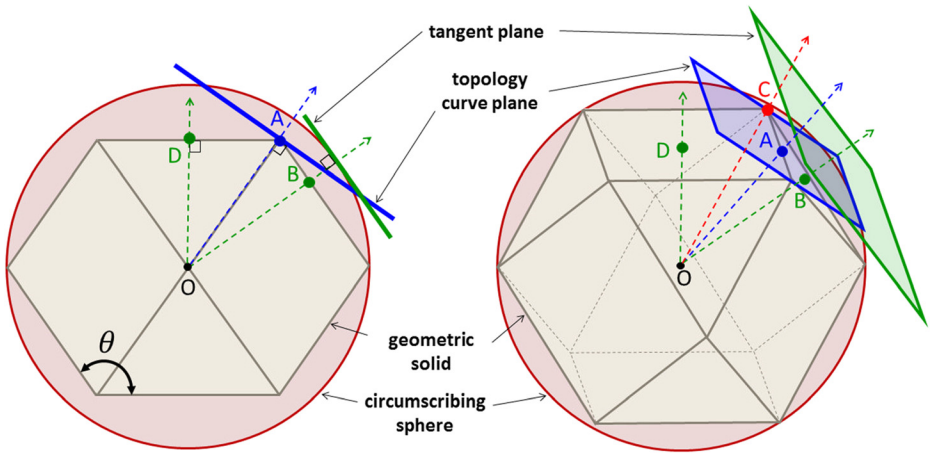

Fig. 5 Cross sectional view of a cuboctahedron containing the origin *O*, the edge midpoint *A*, the vertex *C*, and the face centers *B* and *D*. The face-center-edge angles ϕ_3 and ϕ_4 are $\angle BOA$ and $\angle DOA$, respectively. The face-center-vertex angles β_3 and β_4 are $\angle BOC$ and $\angle DOC$, respectively. The face apothems e_3 and e_4 are defined as $\overline{AB}$ and $\overline{AD}$, respectively. The edge length a is $2\overline{AC}$ and the circum radius R is $\overline{OC}$.

Table 3 Relative apothem lengths for regular polygon faces that occur in Platonic solids

Number of edges per face (p)	Relative apothem length $\frac{e}{a}$
3	$\frac{\sqrt{3}}{6}$
4	$\frac{1}{2}$
5	$\frac{\sqrt{25+10\sqrt{5}}}{10}$

$$\begin{bmatrix}\phi\\ \lambda\end{bmatrix} = \begin{bmatrix}\sin^{-1}\left(\cos(c)\sin(\phi_0)+\dfrac{f(x)\sin(c)\cos(\phi_0)}{\rho}\right)\\ \lambda_0+\tan^{-1}\left(\dfrac{x\sin(c)}{\rho\cos(c)\cos(\phi_0)-f(x)\sin(c)\sin(\phi_0)}\right)\end{bmatrix} = g_0(x,f(x),\phi_0,\lambda_0) \tag{4}$$

where $\rho=\sqrt{x^2+f^2(x)}$ and $c=\sin^{-1}(\frac{\rho}{R})$. The projection origin is then defined as the midpoint of a given p-gon edge as $(\phi_{0,p},0)$. The resulting projection can then be successively rotated $(p-1)$ times about $(0,0)$ by $\frac{2\pi}{p}$ to achieve a spherical module. For a homogeneous forward design, this process will be repeated for each Platonic solid and will result in homogeneous spherical tilings of two different spheres. For a heterogeneous forward design, this process will be repeated for each unique Archimedean face p-gon and will result in heterogeneous tiling of a single sphere. Figure 6 shows the spherical tiling of a cuboctahedron achieved via heterogeneous forward design. While this example shows a tiling where both modules are based on the same MT-curve to achieve perfect spherical tiling, note that both heterogeneous and homogeneous design can use two different MT-curves for the different modules of respective amplitudes A_1 and A_2.

2.5 Planar Topology. The spherical tiles are then projected via azimuthal equidistant projection onto the *tangent plane*. Generically, the resulting planar coordinates (x_p, y_p) for the projection with origin (ϕ_1,λ_1) are given as

$$\begin{bmatrix}x_p\\ y_p\end{bmatrix} = Rk'\begin{bmatrix}\cos(\phi_s)\sin(\lambda_s-\lambda_1)\\ \cos(\phi_1)\sin(\phi_s)-\sin(\phi_1)\cos(\phi_s)\cos(\lambda_s-\lambda_1)\end{bmatrix} = g_1(x,f(x),\phi_0,\lambda_0,\phi_1,\lambda_1) \tag{5}$$

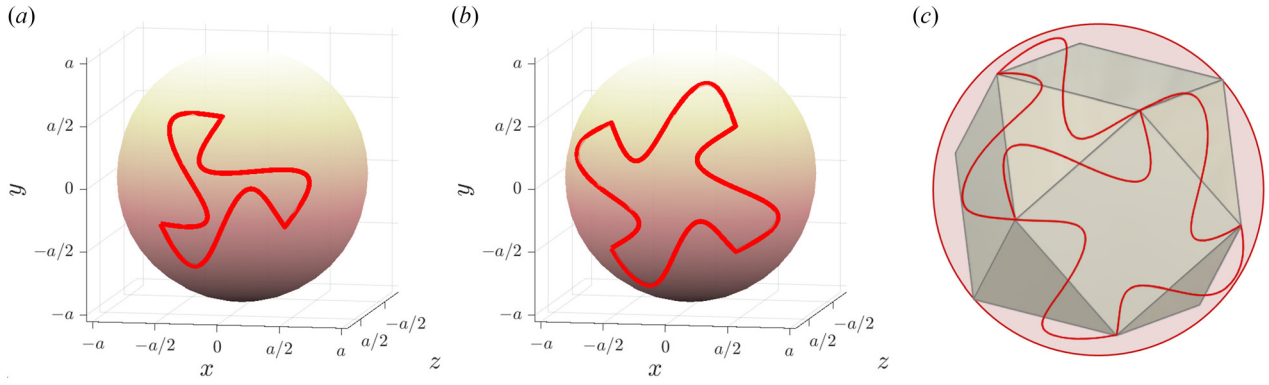

Fig. 6 The cuboctahedron spherical module topologies achieved via heterogeneous forward design with edge length *a* and MT curve amplitude *A* = 0.7. The spherical topology consists of the (*a*) three-limb module and (*b*) four-limb module, which can be combined into (*c*) a CAD rendering of spherical tiling modules for adjacent faces of the cuboctahedron.

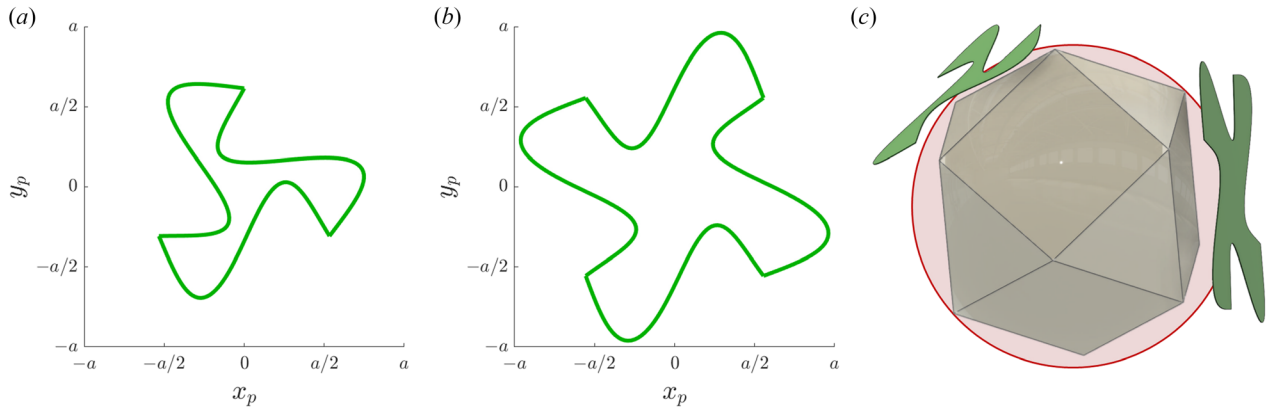

Fig. 7 The cuboctahedron planar module topologies achieved via heterogeneous forward design, shown with (*a*) the three-limb module, (*b*) the four-limb module, and (*c*) a CAD rendering of the planar topologies tangent to the circumscribing sphere for a cuboctahedron

where $k' = \frac{c}{\sin(c)}$ is the scale factor and $\cos(c) = \sin(\phi_1)\sin(\phi) + \cos(\phi_1)\cos(\phi)\cos(\lambda - \lambda_1)$. Because the projection center is defined as the center of the p-gon face, $\phi_1 = \lambda_1 = 0$. Figure 7 displays the planar topology for cuboctahedron-based modules via heterogeneous forward design.

$$\begin{bmatrix} \phi' \\ \lambda' \end{bmatrix} = \begin{bmatrix} \sin^{-1}\left(\cos(c)\sin(\phi'_0) + \dfrac{y_p \sin(c)\cos(\phi'_0)}{\rho}\right) \\ \lambda_0 + \tan^{-1}\left(\dfrac{x_p \sin(c)}{\rho\cos(c)\cos(\phi'_0) - y_p \sin(c)\sin(\phi'_0)}\right) \end{bmatrix} \tag{6}$$

3 Inverse Design for Spherical Reconfiguration

The inverse design process creates new spherical topology based on the planar topology of the forward design. In the case of heterogeneous forward design (based on an Archimedean solid) the inverse design nets multiple unique homogeneous spherical topologies. Inverse design of modules with homogeneous forward design (based on Platonic solids) will result in a single heterogeneous spherical topology. The inverse consists of the projection (Sec. 3.1) with respect to a polyhedron vertex alignment (Sec. 3.2) scaling factor to ensure proper construction. In this section, any variable denoted a sprime ($'$) refers to the inverse topology.

3.1 Inverse Spherical Topology. The inverse spherical topology is obtained through an inverse azimuthal equidistant projection [12] of the planar topology to a sphere of radius $\kappa R'$ determined by the solid type, edge length, and scaling factor κ. The scaling factor is defined in Sec. 3.2. The new longitude and latitude coordinates for projection origin (ϕ'_0, λ'_0) are

where $\rho = \sqrt{x_p^2 + y_p^2}$, $c = \frac{\rho}{R'}$, $\phi'_0 = \phi_{0,p}$ for a p-gon module face, and $\lambda_0 = 0$ (for projection origin centered at the polyhedral edge midpoint).

3.2 Polyhedron Vertex Alignment. The distortion due to the azimuthal equidistant projection results in a spherical configuration that does not align with the polyhedral vertices. The radius for reconfiguration therefore needs to be scaled to ensure polyhedral vertex alignment. The scale invariant design of the modules allows for a constant ratio between the edge lengths (a', a) of the base Platonic solid and Archimedean solid, respectively, for the spherical reconfiguration regardless of the input parameters (a, A). The azimuthal equidistant projection preserves distance radially from the center of projection. Thus, the center-vertex distance of the planar topology equals the center-vertex spherical distance of the forward design, as shown in Fig. 8. However, a scaling factor κ is required to adjust the inverse design radius R' to ensure that this distance aligns with the spherical center-vertex distance of the inverse design. Vertex alignment between solids occurs when

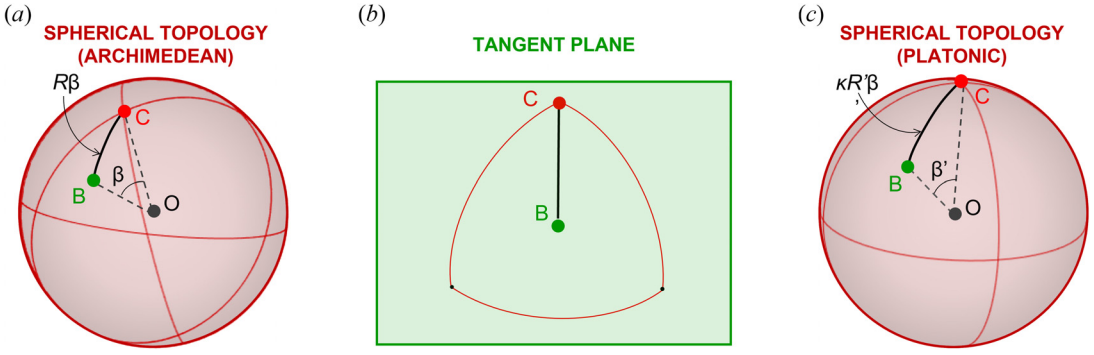

Fig. 8 For heterogeneous forward design, the distance $\overline{BC}$ is equal to (*a*) the spherical distance $R\beta$ on the Archimedean spherical tessellation, (*b*) the center-vertex distance on the planar projection of the tessellation, and (*c*) the spherical distance $\kappa R'\beta'$ in the Platonic spherical tessellation

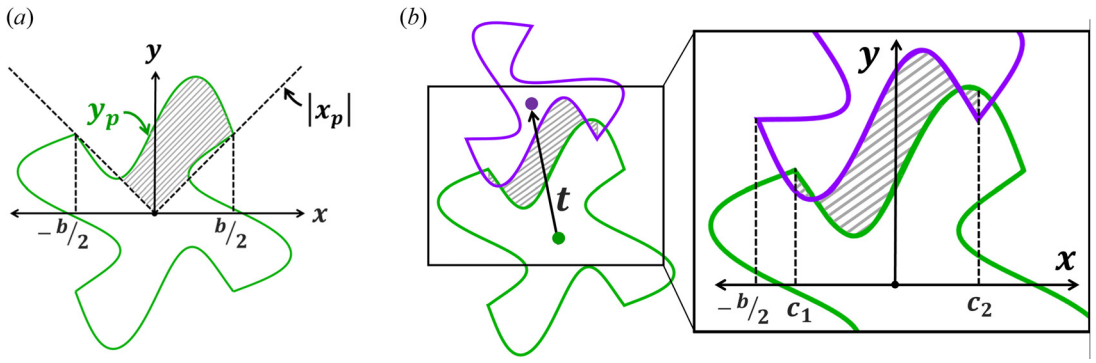

Fig. 9 The planar distortion for the example heterogeneous three-limb module and four-limb module is related to (*a*) the area (shaded) of a module limb bounded by the planar topology curve and the limb sector line, and (*b*) the intermodular area (shaded) between adjacent modules offset by *t*

$$\kappa\left(\frac{R'}{a'}\right)\beta' = \left(\frac{R}{a}\right)\beta \tag{7}$$

where κ is a nondimensional scaling factor.

4 Module Topology Optimization

Module topology optimization for planar and spherical reconfiguration is obtained by minimizing the cost function that is a weighted sum of the planar and spherical reconfiguration distortion metrics. These metrics areas are a function of the amplitude of the module topology curve A. The generic module topology set optimization problem can be written as

$$\begin{aligned}&\left(A_1^*, A_2^*, \ldots A_n^*\right) = \operatorname{argmin} J(A_1, A_2, \ldots A_n) \qquad \text{s.t.} \quad \mathrm{A_i, w} \in [0,1]\\ &\text{where} \quad J(A_1, A_2, \ldots A_n) = w\frac{1}{N_p}\sum_{i=1}^{N_p}\varepsilon_p + (1-w)\frac{1}{N_s}\sum_{j=1}^{N_s}\varepsilon_s\end{aligned} \tag{8}$$

where ε_p and ε_s are the distortion metrics for planar and spherical reconfiguration, respectively, and w is a constant scalar weight. Additionally, n is the number of distinct p-gon face/modules shapes, $N_p = \binom{n}{2}$ is the number of planar distortion metrics, and N_s is the number of spherical distortion metrics where $N_s = n+1$ for heterogeneous forward design and $N_s = 1$ for homogeneous forward design. These values assume that a given p-gon shape is only used for a single corresponding homogeneous reconfiguration profile.

4.1 Planar Distortion Metric. The planar distortion metric ε_p for modules in planar configuration is calculated as

$$\varepsilon_p = \frac{G_p(p_1 + p_2)}{P_1 + P_2} \tag{9}$$

where G_p is the intermodular area (i.e., cavity and/or overlap) between modules, P_j is the total area of module j for $j = \{1, 2\}$, and p_j is the number of edges for the p-gon of module j. For homogeneous configurations $p_1 = p_2$ and $P_1 = P_2$. Distortion metrics are calculated for both homogeneous configurations (e.g., two four-limb modules) and heterogeneous configurations (e.g., a four-limb module and a three-limb module). These areas are displayed in Fig. 9. The area of a single limb is the area between the planar topology curve y_p achieved via forward design and the limb sector line, defined as $|\cot\frac{\pi}{p}|$. The total module area P is then calculated as the area of a single limb times the number of limbs on the module:

$$P = p\int_{-b/2}^{b/2}\left(y_p - \left|\cot\left(\frac{\pi}{p}\right)\right|x_p\right)dx_p \tag{10}$$

where $(-\frac{b}{2}, \frac{b}{2})$ are the projected vertices of the base solid. The intermodular area between one planar module (x_{1p}, y_{1p}) and another (x_{2p}, y_{2p}) is defined with respect to a variable center-to-center offset $\boldsymbol{t} \in [-\frac{b}{8}, \frac{b}{8}]$.

$$G_p = \min_{\boldsymbol{t}}\left(\int_{c_1}^{c_2} y_{1p}(x_{1p})dx_{1p} - \int_{c_1}^{c_2} y'_{2p}(x'_{2p})dx'_{2p}\right) \tag{11}$$

where

$$\begin{bmatrix} x'_{2p} \\ y'_{2p} \end{bmatrix} = \begin{bmatrix} t_x \\ t_y \end{bmatrix} + \begin{bmatrix} \cos(\pi) & -\sin(\pi) \\ \sin(\pi) & \cos(\pi) \end{bmatrix}\begin{bmatrix} x_{2p} \\ y_{2p} \end{bmatrix} \tag{12}$$

For homogeneous configurations, $(x_{1p}, y_{1p}) = (x_{2p}, y_{2p})$ but $(x_{1p}, y_{1p}) \neq (x_{2p}, y_{2p})$ for heterogeneous configurations.

4.2 Spherical Distortion Metric. The spherical distortion metric ε_s relates to the proportion of the spherical surface that needs to deform to create a full sphere with a radius of R. It is defined for modules in a given spherical configuration as

$$\varepsilon_s = E\frac{G_s}{S} \tag{13}$$

where E is the total number of edges for a given circumscribed polyhedron, G_s is the spherical surface intermodular area, and $S = 4\pi R^2$ is the total surface area for a spherical configuration of radius R. The spherical intermodular area G_s is the surface area between two edges of modules in docking position, shown in Fig. 10. *Docking position* indicates that the endpoints of all spherical module edges are aligned with the vertices of the base solid for that configuration. This space is represented by the three-dimensional Euclidean curve T_i, given as

$$\boldsymbol{T_i}(\phi, \lambda) = R\begin{bmatrix} \cos(\phi)\cos(\lambda) \\ \cos(\phi)\sin(\lambda) \\ \sin(\phi) \end{bmatrix} \tag{14}$$

and $\boldsymbol{T'}$, a 180 deg rotation about the midradius (i.e., the line connecting the sphere's center and the polyhedral edge midpoint). If the polyhedral edge midpoint occurs at (0, 0), the midradius aligns with the x-axis and the rotation matrix Q is given as

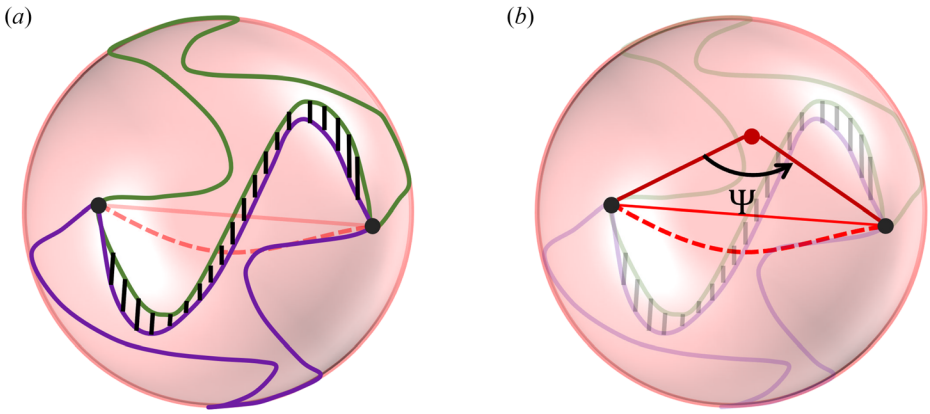

Fig. 10 (*a*) The spherical intermodular area G_s is the shaded surface area between adjacent modules. (*b*) It is calculated by integrating the small arcs (shaded) along the spherical edge Ψ of the base solid.

$$Q = \begin{bmatrix} 1 & 0 & 0 \\ 0 & -1 & 0 \\ 0 & 0 & -1 \end{bmatrix} \tag{15}$$

The rotated curve $\boldsymbol{T}_i' = Q\boldsymbol{T}_i$ represents an adjacent module edge in docking position. The spherical intermodular area can be thought of as a sum of spherical arcs along the projection of the inverse solid edge to the reconfiguration space. The spherical edge for a polyhedron of edge length a has an angular sweep ψ which can be calculated as

$$\psi = 2\cos^{-1}\left(\frac{\sqrt{R^2 - (a/2)^2}}{R}\right) \tag{16}$$

The spherical intermodular area can then be calculated as

$$G_s = \int\int_S d\phi d\lambda = R^2 \int_{-\frac{\psi}{2}}^{\frac{\psi}{2}} \cos^{-1}\left(\frac{\boldsymbol{T_1} \cdot \boldsymbol{T_2'}}{R^2}\right) d\psi \tag{17}$$

Note that for a homogeneous sphere $T_1 = T_2$ and for a heterogeneous sphere $T_1 \neq T_2$.

5 Results

The design methodology was used to generate two sets of hetereogeneous MSoRos in simulation (MATLAB) and model their capability for spherical reconfiguration in both homogeneous (cube and octahedron) and heterogeneous (cuboctahedron) configurations. Using the methods outlined in Sec. 4, reconfiguration distortion metrics for spherical and planar configurations were calculated for modules with MT-curve amplitudes $A_1, A_2 \in [0, 1]$. Areas were calculated using numerical integration with spline interpolation and all optimization was performed using MATLAB's `fmincon`. The resulting cost function J was simulated for varying amplitude values with constant weight factor $w = 0.5$ (equal weighting) for both homogeneous (cube and octahedron bases) and heterogeneous (cuboctahedron bases) forward design. The results (Fig. 11) suggest that the heterogeneous forward design results in lower average overall distortion. Figure 12 plots the individual components of this cost function and highlights the difference between homogeneous and heterogeneous forward design: homogeneous forward design assumes zero distortion in the homogeneous spherical configuration (spherical octahedron and spherical cube) while heterogeneous forward design assumes zero distortion in the heterogeneous spherical configuration (spherical cuboctahedron). Because planar distortions increase radially from the center of the module, modules that constitute a larger surface

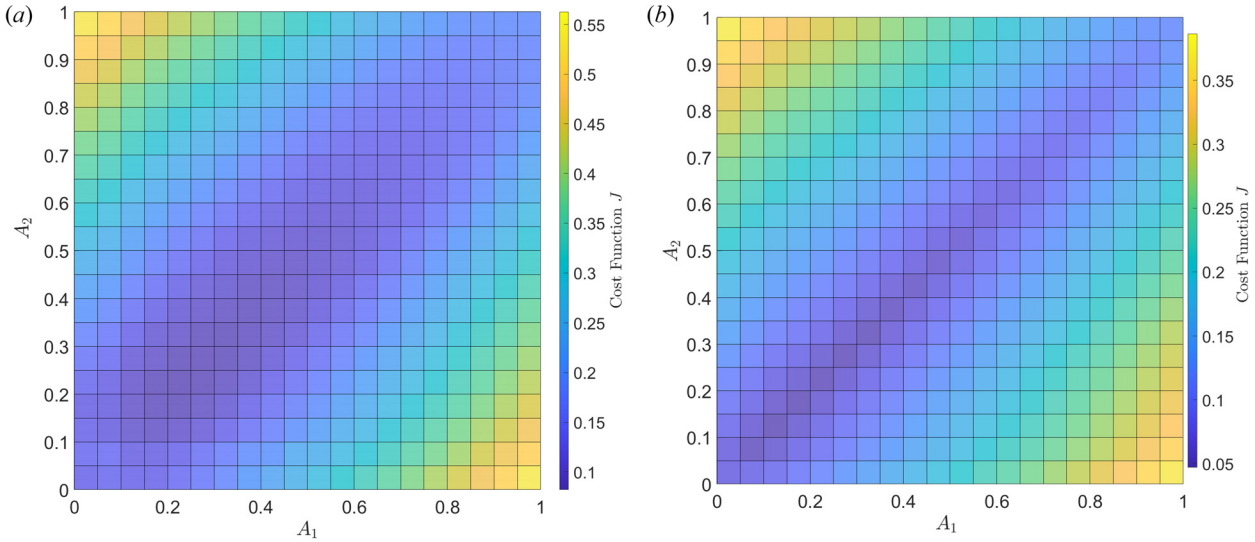

Fig. 11 The weighted sum ($w = 0.5$) of distortion metrics for a cube, octahedron, cuboctahedron heterogeneous-homogeneous module set with (*a*) homogeneous forward design, (*b*) heterogeneous forward design

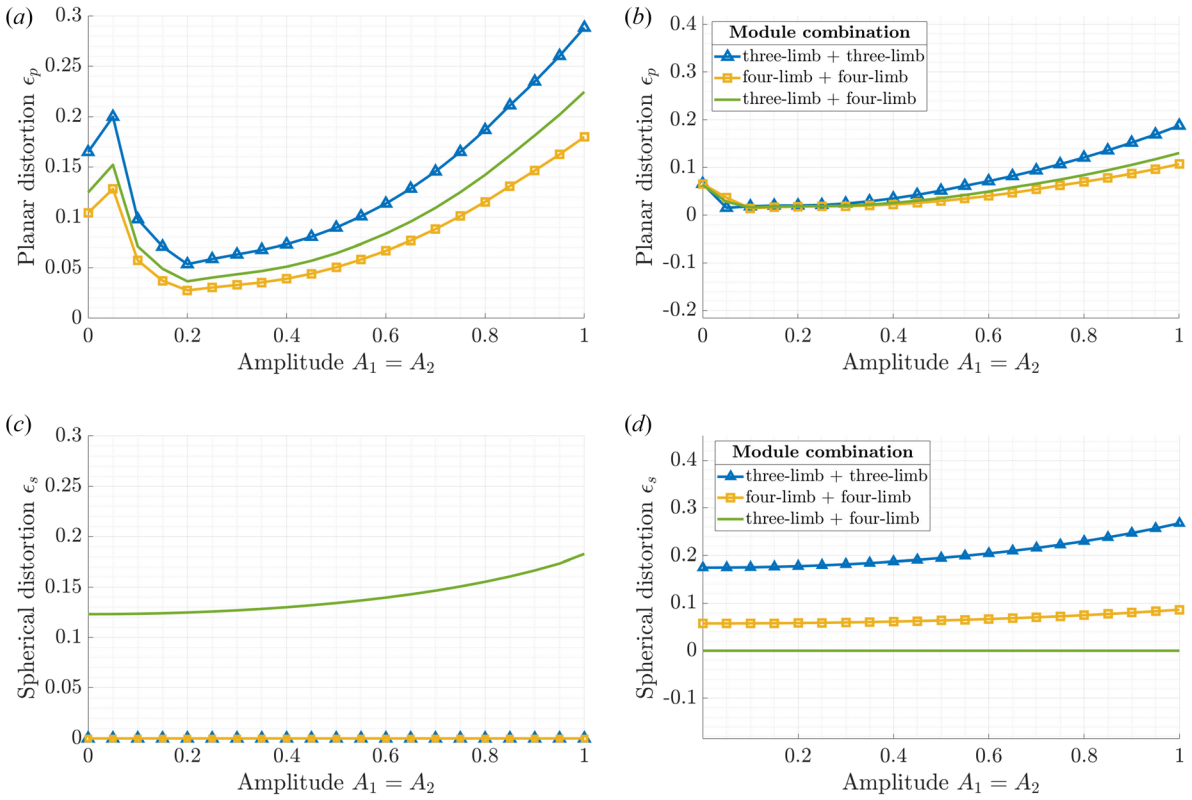

Fig. 12 Individual distortion metrics for cuboctahedron-based modules versus the MT-curve amplitudes. The cost function is composed of a weighted sum of all planar and spherical distortions that occur due to predicted overlaps/cavities between all three combinations of two modules. On the top row, the planar distortion metrics for modules achieved via (*a*) homogeneous and (*b*) heterogeneous forward design are plotted. The bottom row plots the spherical distortion metrics for (*c*) homogeneous and (*d*) heterogeneous forward design.

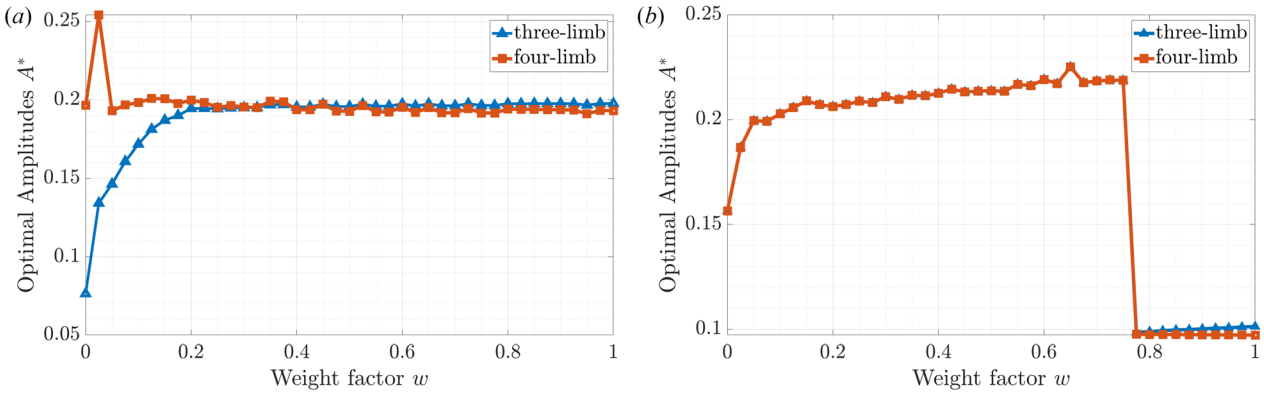

Fig. 13 Optimal MT-curve amplitudes for modules designed via (*a*) homogeneous forward design and (*b*) heterogeneous forward design

area proportion of the sphere will generally result in larger planar distortions. This is reflected in the fact that the homogeneous forward modules have larger planar distortions than the heterogeneous forward modules as the former are based on spheres composed of a smaller number of modules that take up a larger percentage of surface area on the sphere. The difference is pronounced enough to result in lower overall distortion for the heterogeneous first modules when using equal weighting in the cost function.

Simulations were then run with different weighting values w. The optimal MT-curve amplitudes A_i^* for varying weights are shown in Fig. 13. The data suggest that weighting factor does not have a significant effect on optimal design; the optimal curve amplitudes are nearly constant aside from an initial divergence of the homogeneous forward amplitudes when $w < 0.2$ and a sharp drop in heterogeneous forward amplitudes when w exceeds 0.75 (i.e., when planar distortion metrics are treated as more than three times as important as spherical distortion metrics). Furthermore, distortion is minimized when the MT-curve amplitudes of the two modules are approximately equal ($A_1 \approx A_2$) Finally, the results indicate that the heterogeneous forward design generates a lower optimal amplitude and lower distortion metrics, with MT-curve amplitude of $A^* \approx 0.2$. The expected overlap/cavities for adjacent planar and spherical topologies of the optimal three-limb and four-limb MSoRos are visualized in Fig. 14. Interestingly, the heterogeneous forward design leads to cavities in the spherical configurations as opposed to the overlap in the spherical configurations observed in the homogeneous forward design scenario. This distinction may influence the forward design choice.

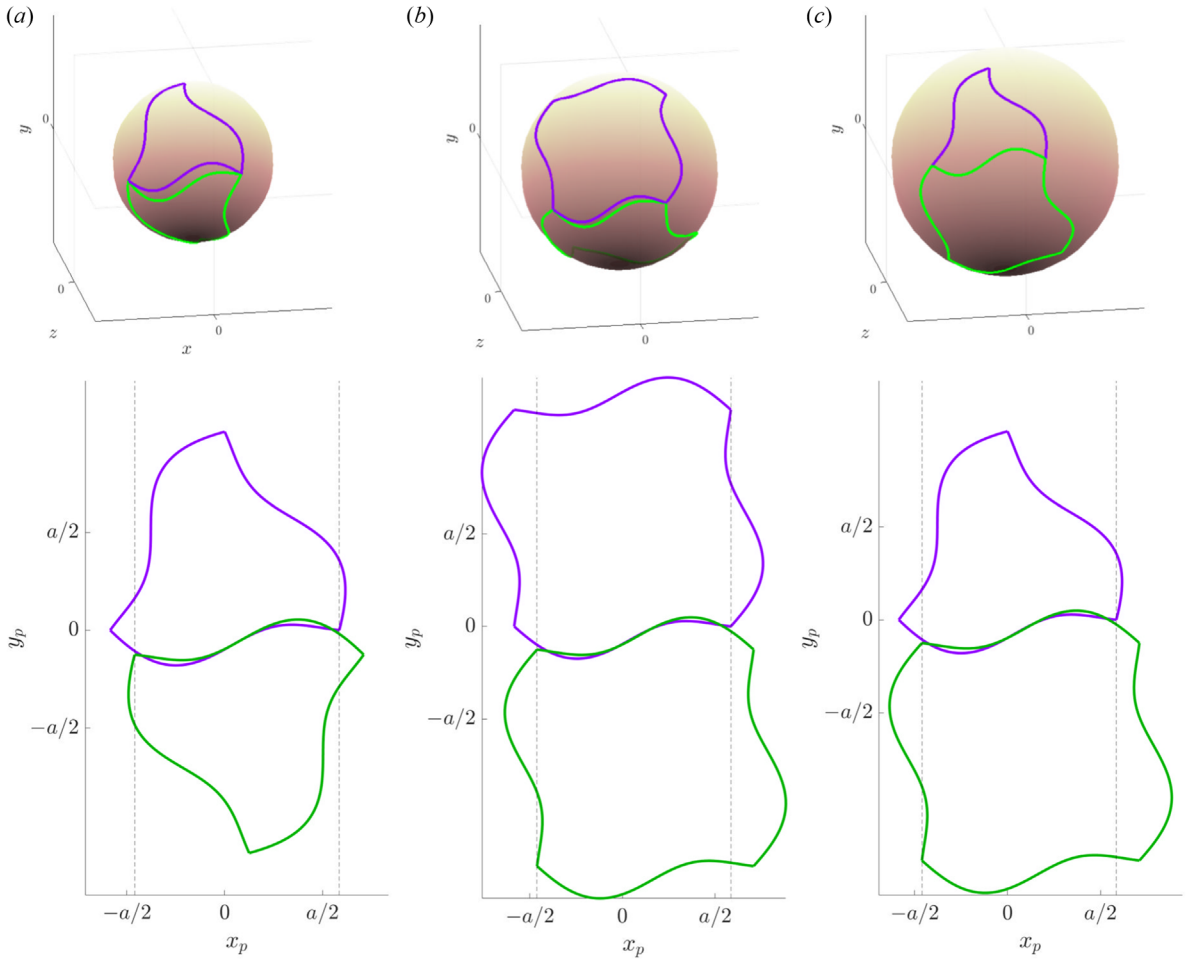

Fig. 14 Optimal cuboctahedron MSoRo topologies achieved via heterogeneous forward design showing the calculated cavities/overlap of the spherical (top) and planar (bottom) modules. The intermodular distortions are shown for (*a*) heterogeneous pairing, (*b*) homogeneous three-limb pairing, and (*c*) homogeneous four-limb pairing.

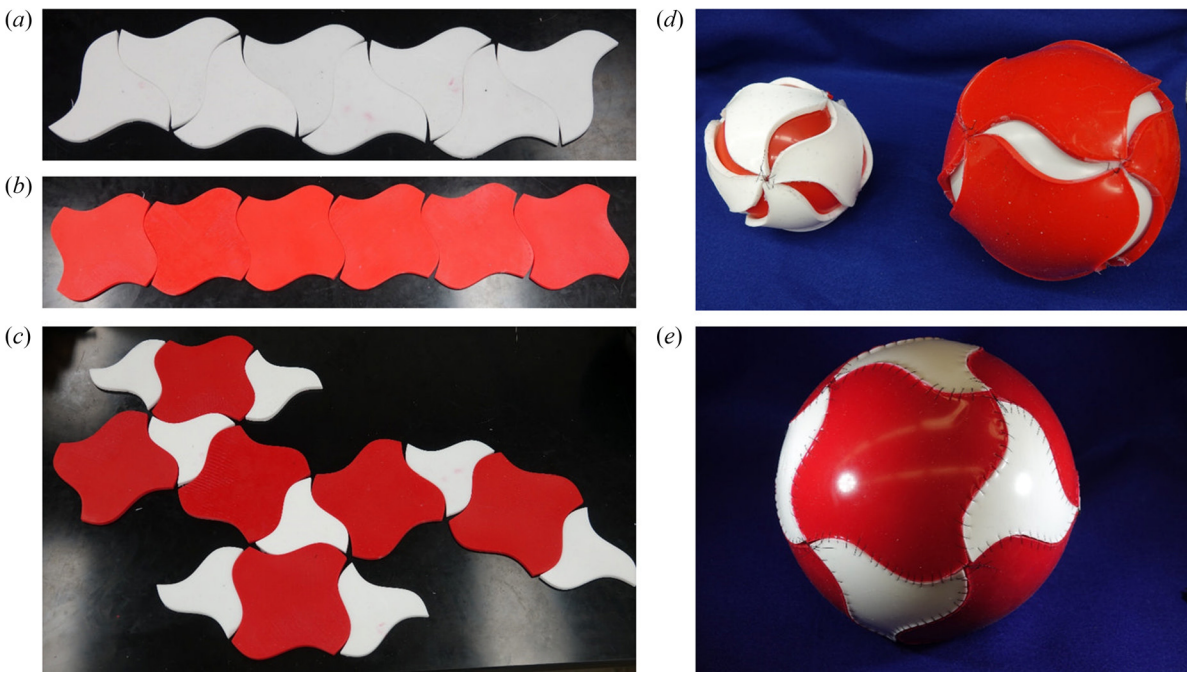

Fig. 15 Experimentally fabricated optimal MSoRo topologies for the three-limb and four-limb MSoRo designed via heterogeneous forward design. These modules have ability perform heterogeneous and homogeneous reconfiguration, showing 1D planar line configurations for (*a*) the eight octahedron modules and (*b*) the six cube modules, (*c*) the 2D planar net configuration for the fourteen cuboctahedron modules, and the 3D spherical configurations for (*d*) the homogeneous octahedron modules (left), the cube (right), and (*e*) the fourteen heterogeneous cuboctahedron modules.

In Fig. 15, the simulation results were validated experimentally by casting thin modules with silicone rubber (Smooth-On Dragon Skin 10) and arranging them in different configurations. It is important to note that the purpose of this fabrication is simply to investigate the surface topology of soft modules and visualize the resulting distortions; therefore, robot morphology, actuation, and docking are not considered here and are instead the subject of future work. As expected, the largest distortions gaps/overlaps occur in the homogeneous spheres (Fig. 15(*d*)).The experimental modules also experience larger spherical gaps due to the thickness of the modules causing "bowing". This can be addressed by optimizing the morphology to encourage spherical curling. Note that the homogeneous spheres in this image are only attached at the vertices (unlike the heterogeneous cuboctahedron module). Therefore, it is expected that a properly designed docking mechanism combined with robot actuation would be able to address this.

6 Conclusion

The research presents a methodology for optimal topology design of versatile MSoRos that can reconfigure between both heterogeneous and homogeneous configurations. As an example, the fourteen MSoRos (six four-limb, eight three-limb) are designed using an Archimedean solid (cuboctahedron) as the base polyhedron. They are capable of spherical heterogeneous reconfiguration amongst themselves (all fourteen modules), and also individually, i.e., six homogeneous four-limb modules or eight three-limb. The generic design process involves choice of the base solid(s) and the module topology curve (MT-curve) that is strategically drawn on the module topology plane. The topology of the robot module in the spherical configuration is obtained through orthographic projection onto a sphere. This topology is subsequently projected onto the tangent plane through an azimuthal equidistant projection. The polyhedron-dependent geometric quantities required for these projections are presented. The optimal topology is then obtained by ensuring alignment of the polyhedron vertices and minimizing the spherical and planar distortions. Such distortion metrics are quantified as the normalized intermodular areas in the spherical and planar configurations. Simulations are performed comparing scenarios where the forward design is based on a set of Platonic solids (homogeneous) or an Archimedean solid (heterogeneous). The results indicate that heterogeneous forward design results in lower overall distortion. However, for both the cases, the optimal amplitudes for the MT-curves are around 0.2. Heterogeneous forward design was favored in this paper due to the smaller planar distortions and ability to minimize distortion in the heterogeneous spherical configuration. Optimal modules from heterogeneous forward design were then fabricated with silicone rubber to validate the simulation results.

As this paper focuses on the surface topology, actuation, robot morphology, and docking are not considered. Therefore, the level to which actual modules can compensate for distortion cannot be conclusively stated. Future work includes the exploration of the cost function (e.g., incorporating locomotion difficulty) and MT-curves outside of the simple sine curve family presented here. Furthermore, docking remains an open problem to be explored.

Nomenclature

a = edge length
A = amplitude
e = apothem length for a face
E = number of edges on a solid
f = module topology curve
F = number of faces on a solid
g_0 = forward design spherical topology
g_1 = planar topology
g_1^{-1} = inverse design spherical topology
G_p = area of planar error
G_s = surface area of spherical error
J = cost function
p = number of edges per face
P = area of planar modules
q = number of faces per vertex
Q = rotation matrix
R = circum radius
S = surface area of a sphere
$\boldsymbol{t}$ = parameterized spherical topology
w = weight of spherical error in the cost function
x = domain of module topology curve
x_p = x-values of planar topology
y_p = y-values of planar topology
β = vertex angular offset
κ = scale factor for side length
λ = longitude
ε_p = planar distortion metric
ε_s = spherical distortion metric
ϕ = latitude
ϕ_0 = edge angular offset
ψ = angular sweep of a spherical polyhedron edge

References

[1] Yim, M., Duff, D. G., and Roufas, K. D., 2000, "PolyBot: A Modular Reconfigurable Robot," IEEE International Conference on Robotics and Automation (ICRA), Vol. 1, San Francisco, CA, Apr. 24–28, pp. 514–520.
[2] Lee, W. H., and Sanderson, A. C., 2002, "Dynamic Rolling Locomotion and Control of Modular Robots," IEEE Trans. Rob. Autom., **18**(1), pp. 32–41.
[3] Kurokawa, H., Tomita, K., Kamimura, A., Kokaji, S., Hasuo, T., and Murata, S., 2008, "Distributed Self-Reconfiguration of M-TRAN III Modular Robotic System," Int. J. Rob. Res., **27**(3–4), pp. 373–386.
[4] Sastra, J., Chitta, S., and Yim, M., 2009, "Dynamic Rolling for a Modular Loop Robot," Int. J. Rob. Res., **28**(6), pp. 758–773.
[5] Seo, J., Paik, J., and Yim, M., 2019, "Modular Reconfigurable Robotics," Annu. Rev. Control, Rob., Auton. Syst., **2**(1), pp. 63–88.
[6] Yim, M., Zhang, Y., and Duff, D., 2002, "Modular Robots," IEEE Spectrum, **39**(2), pp. 30–34.
[7] Yim, M., Shen, W., Salemi, B., Rus, D., Moll, M., Lipson, H., Klavins, E., and Chirikjian, G. S., 2007, "Modular Self-Reconfigurable Robot Systems [Grand Challenges of Robotics]," IEEE Rob. Autom. Mag., **14**(1), pp. 43–52.
[8] Yim, M., White, P., Park, M., and Sastra, J., 2009, "Modular Self-Reconfigurable Robots," *Encyclopedia of Complexity and Systems Science*, Springer, Berlin, pp. 5618–5631.
[9] Onal, C. D., and Rus, D., 2012, "A Modular Approach to Soft Robots," 4th IEEE RAS EMBS International Conference on Biomedical Robotics and Biomechatronics (BioRob), Rome, Italy, June 24–27, pp. 1038–1045.
[10] Kwok, S. W., Morin, S. A., Mosadegh, B., So, J.-H., Shepherd, R. F., Martinez, R. V., Smith, B., Simeone, F. C., Stokes, A. A., and Whitesides, G. M., 2014, "Magnetic Assembly of Soft Robots With Hard Components," Adv. Funct. Mater., **24**(15), pp. 2180–2187.
[11] Laschi, C., Mazzolai, B., and Cianchetti, M., 2016, "Soft Robotics: Technologies and Systems Pushing the Boundaries of Robot Abilities," Sci. Robot., **1**(1), p. eaah3690.
[12] Snyder, J. P., 1982, "Map Projections Used by the U.S. Geological Survey," U.S. Government Printing Office, Report, pp. 5–10, 135–185.
[13] Yen, J., and Séquin, C., 2001, "Escher Sphere Construction Kit," Proceedings of the 2001 Symposium on Interactive 3D Graphics, I3D'01, Association for Computing Machinery, Chapel Hill, NC, Mar. 26–29, pp. 95–98.
[14] Delp, K., and Thurston, B., 2011, "Playing With Surfaces: Spheres, Monkey Pants, and Zippergons," Proceedings of Bridges 2011: Mathematics, Music, Art, Architecture, Culture, R. Sarhangi and C. H. Séquin, eds., Tessellations Publishing, Coimbra, Portugal, July 27–31, pp. 1–8.
[15] Chen, F., and Wang, M. Y., 2020, "Design Optimization of Soft Robots: A Review of the State of the Art," IEEE Rob. Autom. Mag., **27**(4), pp. 27–43.
[16] Freeman, C., Maynard, M., and Vikas, V., 2023, "Topology and Morphology Design of Spherically Reconfigurable Homogeneous Modular Soft Robots," Soft Rob., **10**(1), pp. 52–65.